Annals of Nuclear Energy 204 (2024) 110539

Contents lists available at ScienceDirect

Annals of Nuclear Energy

journal homepage: www.elsevier.com/locate/anucene

Hydrogen uptake of zirconium alloys in defective fuel rods: Experiment and numerical model

P. Szabó *, Z. Hózer, E. Perez-Feró, T. Novotny

Centre for Energy Research (EK), Konkoly-Thege Miklós út 29-33, Budapest 1121, Hungary

ARTICLE INFO

Keywords:
Defective fuel rods
hydrogen uptake by Zr

ABSTRACT

Hydrogen uptake in defective fuel rods by Zr cladding plays an important role in both cladding embrittlement and internal gas pressure build up. The computer codes need models based on representative experimental data in order to predict correctly the behaviour of defective rods under different conditions.

Isothermal H uptake tests at 300 °C, 330 °C, 370 °C and 400 °C were carried out with Zircaloy-4 and E110 cladding samples. Hydrogen uptake increased with the increase of temperature and significant differences were found between the two alloys. The experimental data on Zircaloy-4 have already been used for the simulation of defective fuel rods in the framework of the EU R2CA project. New correlation was created for E110 cladding, which reproduced well the measured data and which can be introduced into fuel behavior computer codes.

1. Introduction

In case of steam generator tube rupture events the defective fuel rods may provide significant activity release into the primary coolant (Lewis et al., 1997). Furthermore, the mechanical loads associated with the accident conditions can cause further degradation of the fuel rods (Olander et al., 1999; Une et al., 1995) as a consequence of the following phenomena:

- The primary coolant may enter the defective fuel rods after the formation of defect.
- Hydrogen can be produced inside of the fuel rod as from water by different mechanism (radiolysis, corrosion).
- The hydrogen will be accumulated in the gas volume of fuel rod and a part of the available hydrogen will be absorbed by the zirconium cladding tube.
- The high local hydrogen content in some parts of the cladding can create hydride blusters and at those positions the cladding becomes very brittle.
- The change of pressure in the primary coolant and/or in the fuel rod will result in stresses that can lead to secondary failure of the fuel rod.

The understanding and detailed numerical modelling of the above listed phenomena need experimental data, which are representative for the physical parameters of the nuclear power plants.

The high hydrogen content in the cladding represents a safety issue, since it may result in brittle failure of the fuel rod in the reactor (Suman et al., 2015). The hydrogen uptake may happen not only in defective fuel rods, but also with intact fuel due to waterside corrosion (Ensor et al., 2017). In case of accident conditions, the high temperature oxidation of Zr alloys in steam is also accompanied with hydrogen uptake (Steinbrück, 2004).

The hydrogen uptake of cladding materials in nuclear power plants was addressed in several test series. Early studies indicated that the hydrogen uptake of Zr significantly accelerates with the increase of temperature and the existence of oxide film on the metallic surface may slow down the hydrogen uptake process (Gulbransen and Andrew, 1954). The different Zr alloys used in nuclear reactor are characterized by different H pickup fraction and kinetics (Couet et al., 2013; Cox, 1999). The Halden reactor experiments simulated the secondary degradation in defective fuel and illustrated that the significant amount of the hydrogen produced from water inside of the fuel rod can be picked up by the cladding (Wright et al., 2017).

The numerical models of hydrogen uptake take into account the partial pressure of hydrogen in the atmosphere and the amount of absorbed hydrogen in the metal (Große et al., 2008; Veshchunov and Shestak, 2012). The rate of hydrogen uptake strongly depends on temperature (Steinbrück, 2004; Veshchunov and Shestak, 2012). Some transient fuel behavior codes have detailed models for hydrogen

* Corresponding author.
E-mail address: szabo.peter@ek-cer.hu (P. Szabó).

https://doi.org/10.1016/j.anucene.2024.110539
Received 18 August 2023; Received in revised form 15 December 2023; Accepted 9 April 2024
Available online 15 April 2024

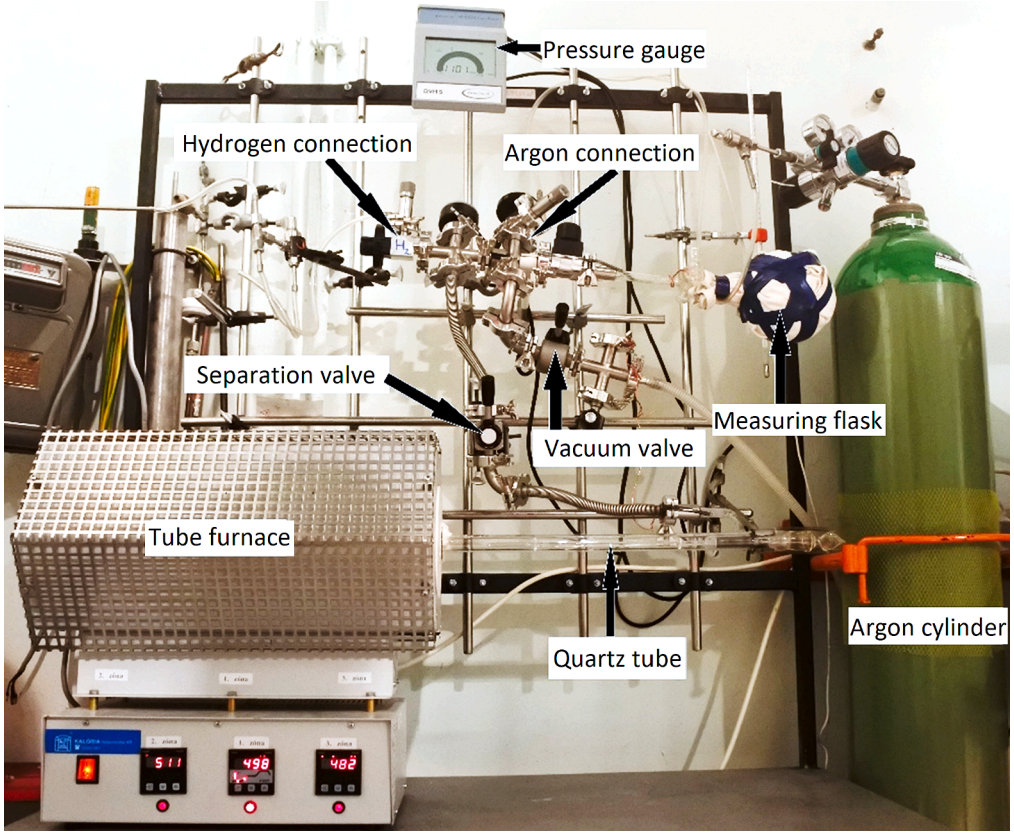

Fig. 1. The equipment used for the Zircaloy-4 and E110 sample hydrogenation.

migration in the cladding and takes into account the terminal solid solubilities for dissolution and for precipitation (Seo et al., 2021).

In the present work the hydrogen uptake of Zr alloys was investigated. There is a large number of tests available on hydrogen uptake of Zr (Steinbrück, 2004; Hatano et al., 1996; Novotny et al., 2015; Grosse et al., 2011), but most of them were carried out at high temperatures. In the defective fuel rods, during normal operational conditions the typical cladding temperatures are in the range of 300–400 °C. In the framework of the EU R2CA project, hydrogen uptake tests have been carried out Zircaloy-4 and E110 cladding tube samples between 300 and 400 °C in the laboratories of Centre for Energy Research, Hungary in order to support the development and validation of numerical models.

In the reality the hydrogen uptake is accompanied with the corrosion of Zr in steam/water. In the present test series – in order to support model development – it was intended to determine the uptake rate in pure hydrogen, without the corrosion effect.

The present paper describes the experimental program of Centre for Energy Research (EK), Hungary carried out with Zircaloy-4 and E110 cladding tube samples. The second part of this report gives a short description of a numerical model which is based on the results of the H uptake tests.

2. Test facility and sample preparation

The sample preparations and the tests were carried out in the laboratories of the Centre for Energy Research.

2.1. Test facility

The experimental set-up consists mainly of an electrically heated three-zone tube furnace with a quartz tube put in it that connects to pipe-line system. The quartz tube contains the sample holder, and can be vacuumed or filled up with argon or hydrogen gas. The pressure of the gas system was measured by a Vacuubrand type DVR 5 pressure gauge and recorded by a computer. The experimental set-up used for hydrogenation of Zr claddings is shown in Fig. 1. while the schematic view of the equipment can be seen in Fig. 2.

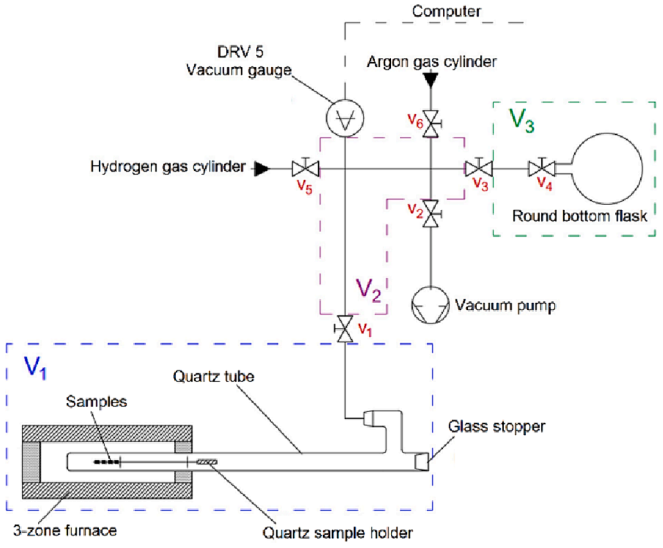

Fig. 2. The schematic view of the equipment for hydrogenation.

The exact volume of the round bottom glass flask was determined to calculate the V_2 volume (see Fig. 2). While V_2 volume has a role in calculating the amount of hydrogen, the exact volume of V_1 is not needed to be determined for the calculations.

Fig. 3. The 8 mm long ring samples (on the left side) placed on the sample holder containing a soft iron core (on the right side).

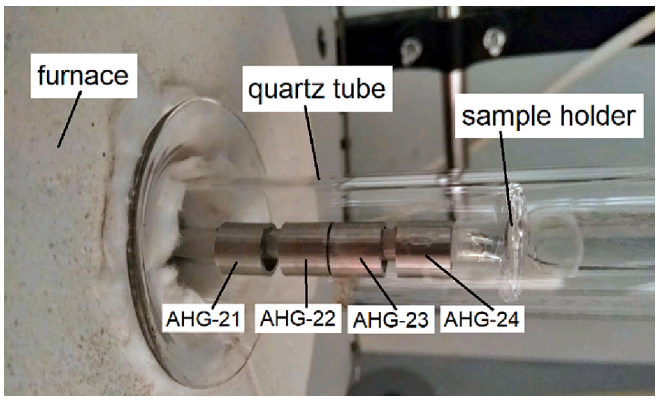

Fig. 4. Sample arrangement on the sample holder.

2.2. Tested materials, sample preparation

The investigated cladding materials were E110 (outer diameter: 9.10 mm; wall thickness: 0.67 mm) and Zircaloy-4 (outer diameter: 10.75 mm, wall thickness: 0.73 mm) alloys. The cladding tubes were cut into 8 mm long specimens. The specimens were open tube segments. Prior to the experiments the tube segments were degreased and cleaned by acetone in ultrasonic bath and weighted carefully.

The samples were weighed both before and after the hydrogenation using a Mettler Toledo XP2U type ultra microbalance having a readability of 0.1 μg.

2.3. Hydrogenation and H content measurements

After cleaning, 4 ring samples were placed on the quartz sample holder (see Fig. 3) that was put into the cold part of the quartz tube outside the furnace.

The samples were always placed on the sample holder in ascending order by their names (e.g. from AHG-21 on the left side to AHG-24 on the right side), and consequently the samples with higher number in their names were placed closer to the outer part of the quartz tube (Fig. 4).

At the cold end of the tube perforated plastic cylinders containing anhydrous calcium-sulphate were placed to adsorb the residual moisture after vacuuming. The tube was closed with a greased (Apiezon L type ultra high vacuum grease) glass stopper.

To remove the air and moisture from the quartz tube, volumes V_1 and V_2 were vacuumed and flushed using ultra high purity grade (99.999 % (5 N)) argon and hydrogen gases. In the end of this process the whole pipeline system was vacuumed.

In the next step the volume V_2 was filled up to 1000 mbar with 5 N pure hydrogen gas. Then the sample holder was pulled into the furnace using a magnet, so the samples got into the hot end of the quartz tube in the furnace, while the right part of the sample holder on Fig. 3 with the soft iron core remained out of the furnace. After 5 min the temperature of the samples reached the target temperature and valve V_1 was opened. The pressure in the ($V_1 + V_2$) volume decreased to a value around 410 mbar. The pressure was continuously measured by the pressure gauge and recorded by a computer during the 23-hour long hydrogenation.

The decreasing of the pressure meant the samples were absorbing the hydrogen. The rate of the pressure decrease was getting lower and lower as an equilibrium was forming between the hydrogen content of the samples and the gas.

After 23 h the recording of the pressure was stopped and the sample holder was fully pulled out from the furnace. After it cooled down to room temperature the system was filled up to around 1000 mbar with argon gas and opened, then the samples were carefully collected and weighed.

The recording of the pressure was started when the pressure dropped from 1000 mbar to around 400–410 mbar after opening valve V_1 (see Fig. 2).

The mass gain of the ring samples is determined by weighing the samples before and after the hydrogenation. Based on the weight of the samples the approximate hydrogen content of the samples can be estimated using the formula:

$$c_{H_i} = \frac{\Delta m}{m_i} \cdot 10^6$$

where:

c_{H_i} hydrogen content (however the effects of the possible oxidation are also included) (ppm).

Δm mass gain of the sample during hydrogenation (grams).

m_i mass of the sample before hydrogenation (grams).

The amount of the hydrogen absorbed by all the four samples can be calculated as follows. The total mass of the hydrogen in volume V_2 before the hydrogenation can be determined by the ideal gas law as we know the V_2 volume, the temperature and the pressure of the hydrogen gas in the volume V_2. The ratio of the absorbed gas to the total amount of it can be determined based on the pressure ratio of the hydrogen gas measured at the beginning and at the end of the experiment. Knowing the total mass of the 4 samples the average absorbed hydrogen concentration can be calculated (in ppm) since the absorption of the hydrogen is not even among the four samples in the furnace.

The quantitative analysis of the hydrogen absorbed in the samples was carried out using an ELTRA ELEMENTRAC OH-p 2 type elemental analyzer. This device uses the hot extraction method and can be used for quick measurement of oxygen and hydrogen concentrations in inorganic samples like steel, iron, copper, zirconium, titanium, molybdenum, nickel or ceramics. The highly sensitive nondispersive infrared (NDIR) and thermal conductivity detectors (TCD) can reliably detect element concentrations from low ppm content to high percentages.

The device consists of two units, the analyzer that includes the high furnace and a cooling unit. The hydrogen concentrations are determined by a robust and sensitive thermal conductivity cell. The sample falls through three airlocks into a graphite crucible, where it is melted by the high temperature generated by the flow of current through the graphite crucible. To decrease the melting point, the small pieces cut out from different positions of the ring samples and weighed before the measurement are placed in nickel capsules and put into the sample holder of the device. The carrier gas is high purity (99.999 %) nitrogen that purges the hydrogen released from the sample to the thermal conductivity cell.

The thermal conductivity detector detects the difference in thermal conductivity between effluent flow (carrier gas + hydrogen) and a reference flow of carrier gas alone; it produces a voltage proportional to this difference. During the measurement the TCD signal is continuously recorded and the differences are finally integrated and converted into hydrogen content (Manual ELTRA ELEMENTRAC ONH-p series. 2017).

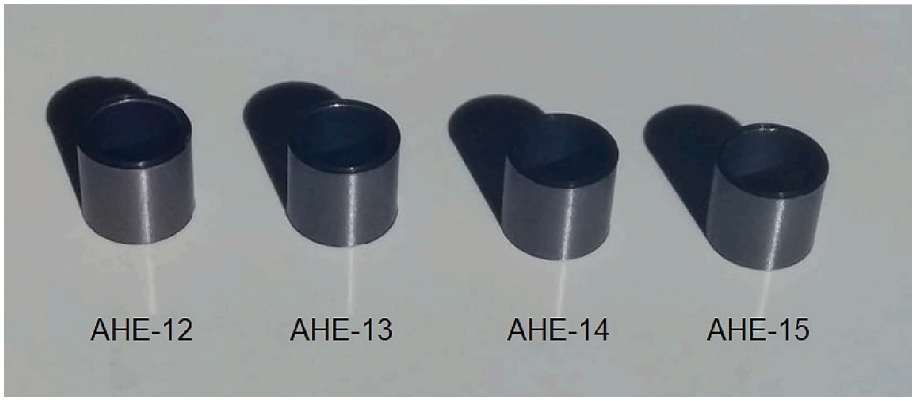

Fig. 5. The gray oxide layer on the samples resulted by the undesired oxidation during the hydrogenation.

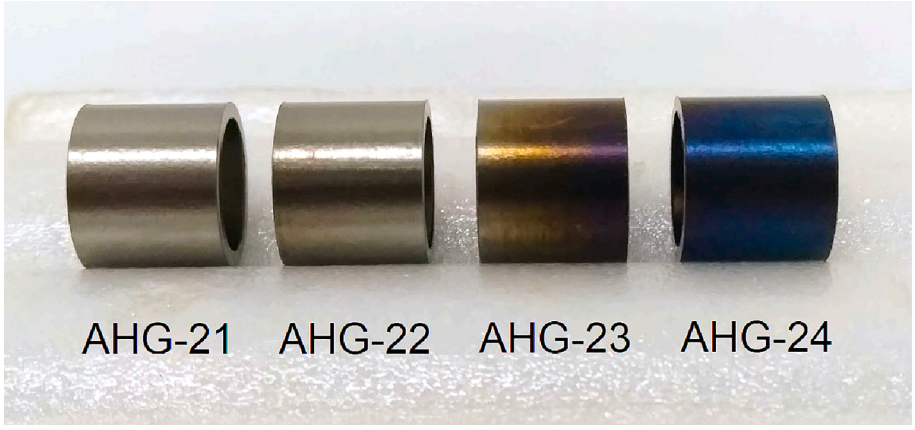

Fig. 6. The colored oxide layer on the outer samples (on the right side) hydrogenated at 330 °C.

3. Results of H uptake tests

The rate and the characteristics of hydrogen uptake of the two alloys were determined at 300 °C, 330 °C, 370 °C, and 400 °C; using 4 ring samples at every temperature. The effect of the temperature on the hydrogen uptake of the two zirconium alloys was also investigated in the range of 300–400 °C.

3.1. Execution of tests

Notwithstanding the presence of the calcium-sulphate getter placed at the joint of the quartz tube, some water vapour (and oxygen) could enter the system during the measurements, and thus slight oxidation of the samples occurred resulting thin oxide layer on the surface of some samples.

Depending on the circumstances (mainly on the temperature and the alloy type) once an oxide layer was formed, it was either dark gray or colourful (if very thin).

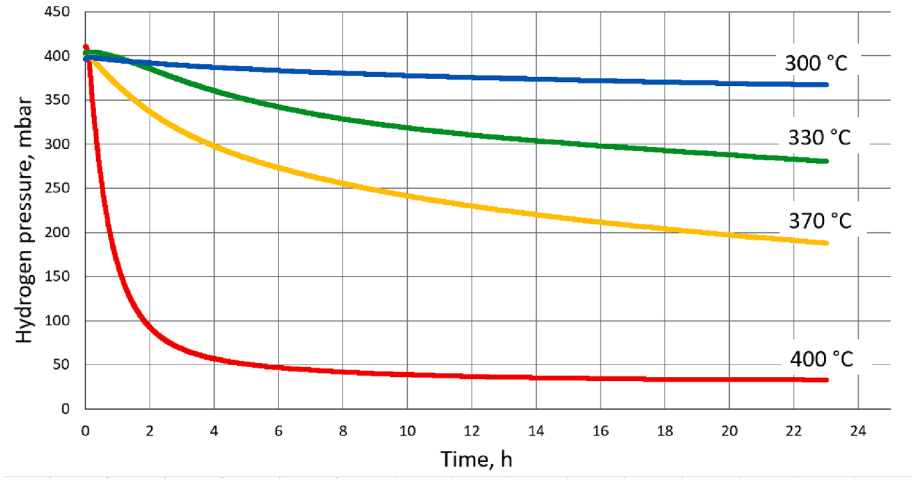

Fig. 7. The hydrogen pressure during the experiments with E110 samples at different temperatures.

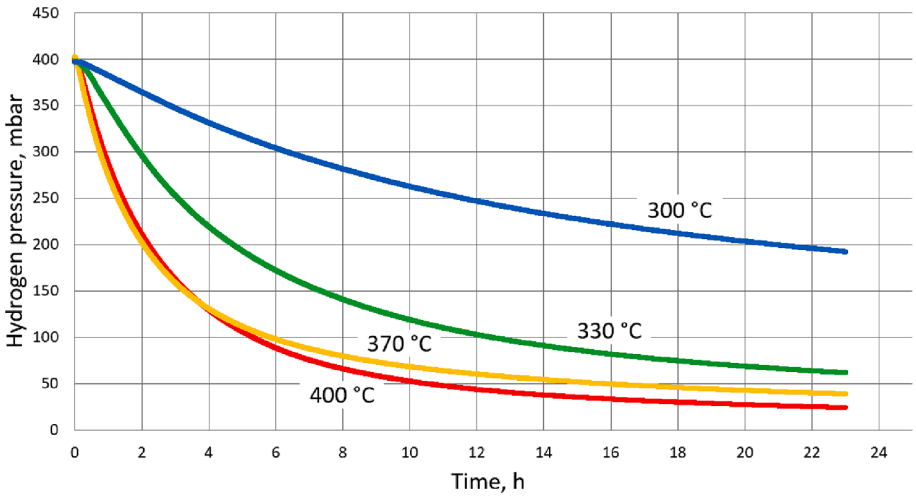

Fig. 8. The hydrogen pressure during the experiments with Zircaloy-4 samples at different temperatures.

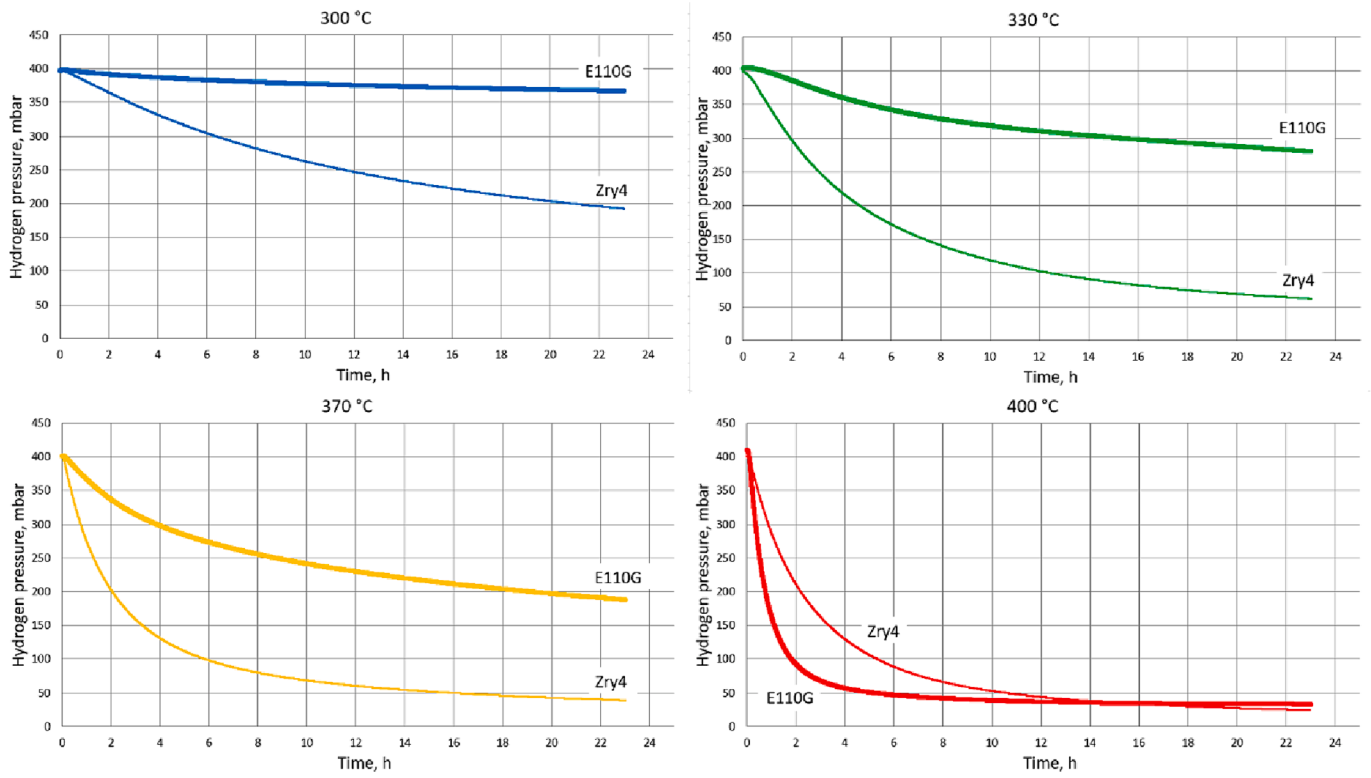

Fig. 9. The difference in the characteristic of the hydrogen uptake between the two alloys at different temperatures.

After the measurement of the samples AHE-12_15 (carried out at 400 °C) an even dark gray oxide layer could be seen on the samples (see Fig. 5). The samples shown in Fig. 5 follow the order like before (i.e. lowest number nearest to the furnace).

At lower temperatures thinner oxide layers occurred on some samples. It can be seen in Fig. 6 that the sample AHG-24 (placed nearest to the outer part of the quartz tube) has a blue oxide layer while the color of the oxide layer on the sample next to it (AHG-23) varies from purple to yellow depending on the rate of the oxidation. The maximum oxide layer thickness was below 1 μm.

The oxygen and water vapour diffused from the outer part of the system did react with the sample AHG-24 first, and thus, this sample has the thickest oxide layer on it. The color and the thickness of the oxide layer indicate how much oxygen and water have been consumed by the reactions with the samples. The inner two rings (AHG-21 and AHG-22) did not suffer visible oxidation, and thus, they remained shiny.

3.2. *Hydrogen uptake results*

The hydrogen uptake of the samples was determined by measuring the hydrogen pressure. Fig. 7 shows the hydrogen pressure as a function of time of hydrogenation in the case of the E110 samples at different temperatures. It can clearly be seen that the higher the temperature is the higher the ratio of the absorbed hydrogen is.

We can see that only around 8 % of the hydrogen has been absorbed by the E110 samples at 300 °C after 23 h while this ratio is 92 % at 400 °C. These ratios are 51 % and 94 % for the Zircaloy-4 alloy samples, respectively (see Fig. 8).

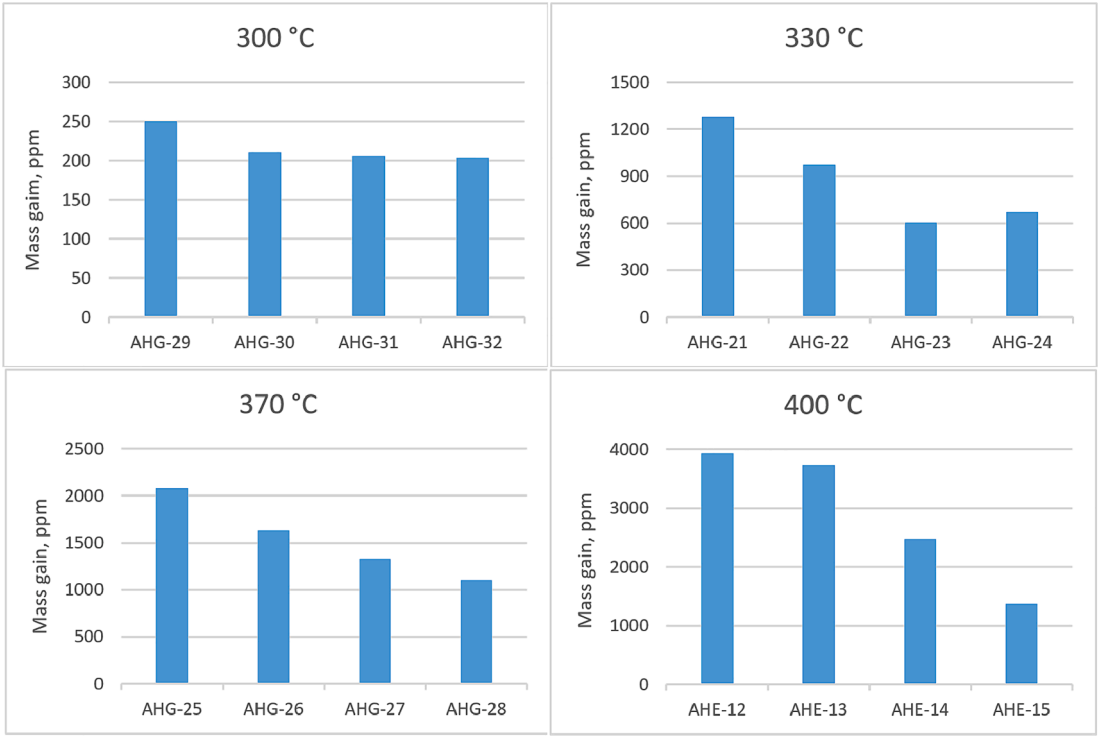

Fig. 10. Mass gain results for the E110 samples.

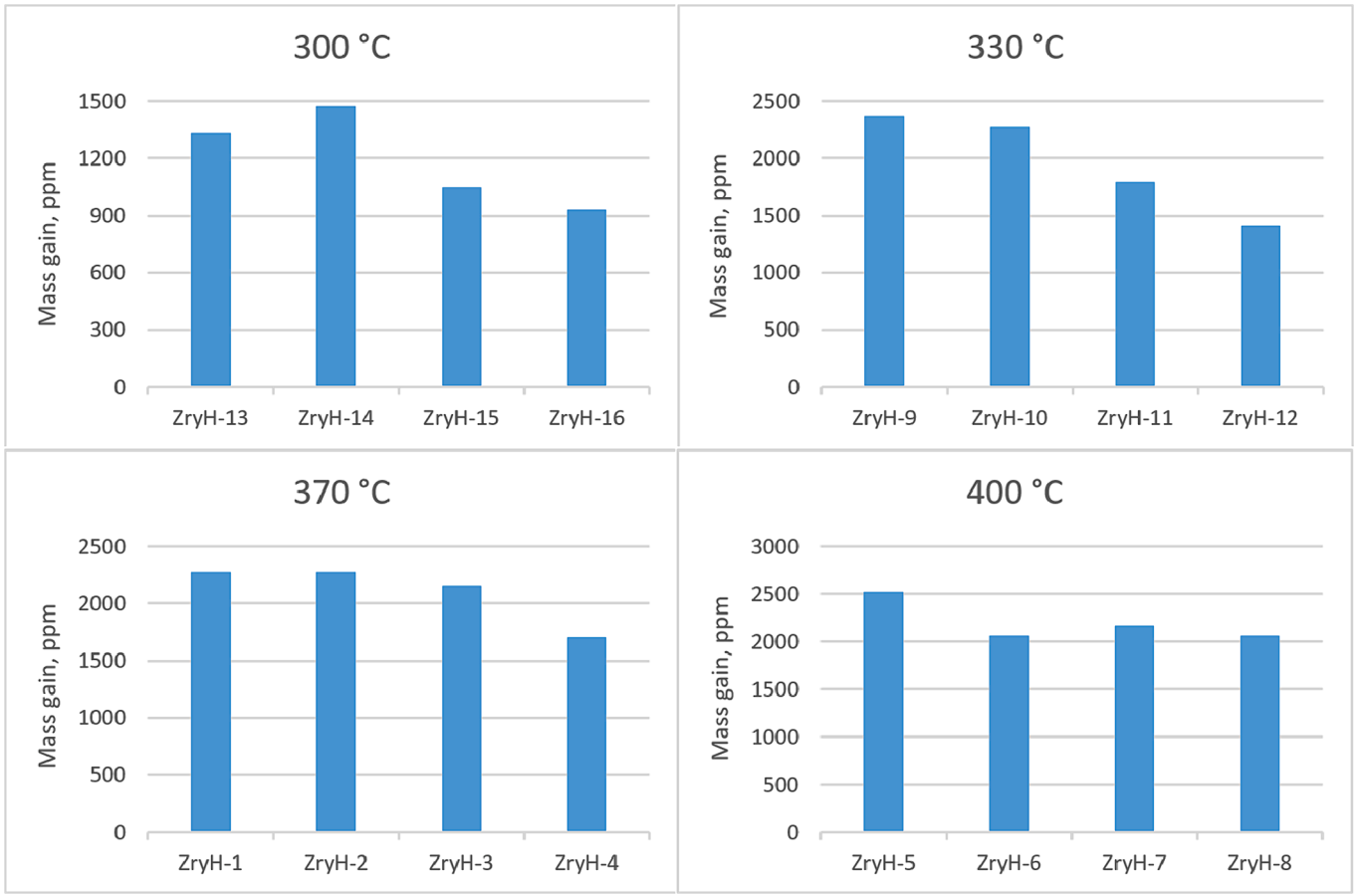

Fig. 11. Mass gain results for the Zircaloy-4 samples.

Table 1
Comparison of the mass gain and the calculated average hydrogen content results.

Temp. (°C)		E110	difference (ppm)	difference (%)	Zircaloy-4	difference (ppm)	difference (%)
300	H content* (ppm)	221.0	3.3	1.49	1203.0	5.9	0.49
	mass gain (ppm)	217.7			1197.1		
330	H content* (ppm)	907.0	25.6	2.82	1980.0	18.2	0.92
	mass gain (ppm)	881.4			1961.8		
370	H content* (ppm)	1556.0	20.6	1.32	2129.0	28.4	1.33
	mass gain (ppm)	1535.4			2100.6		
400	H content* (ppm)	2746.0	133.3	4.85	2188.0	17.8	0.81
	mass gain (ppm)	2879.3			2205.8		

aa* H content determined on the basis of pressure change.

It can be concluded that the ring samples made of E110 alloy do absorb only a small part of the total hydrogen at 300 °C and this ratio is increasing around evenly at higher temperature values. We found this ratio to be ca. 90 % after 8 h at 400 °C and not to increase much thereafter (see on Fig. 7). In the case of the Zircaloy-4 samples the ratio of the absorbed hydrogen was more than 50 % at 300 °C, and this ratio exceeded 80 % already at 330 °C (unlike the case of E110) as well as it did not increase much at higher temperatures (Fig. 8).

Comparing the two alloys' hydrogen uptake at different temperatures we can see that at 300 °C, 330 °C and 370 °C the E110 samples showed lower tendency to absorb hydrogen (Fig. 9), however at 400 °C the pressure decrease was quicker in the experiment with the E110 alloy.

The E110 samples absorbed 90 % of the hydrogen gas already after 8 h while the Zircaloy-4 samples did the same only after 13 h however the Zircaloy-4 samples absorbed a little more hydrogen during the 23-hour long experiment than the samples made of E110 alloy.

The different corrosion behavior of different Zr alloys is well known for long time (Szabó et al., 2017). These differences can be also observed in term of hydrogen pickup. According to a detailed study (Couet et al., 2013), the presence of Nb in the Zr alloy (which is the main alloying element of E110, but not available in Zircaloy-4) and the second-phase precipitates may have a significant effect on the hydrogen pickup. So probably the different composition of E110 and Zircaloy-4 is the main cause of the differences observed in the present tests.

3.3. Mass gain results

The ring samples were weighed (see section 2.3.) and mass gain values were calculated. The mass gain was resulted both by the absorbed hydrogen and by the slight oxidation of the samples. An oxide layer on the surface of a sample reduces the hydrogen absorption rate, and thus, the amount of the hydrogen that can be absorbed. Usually thicker oxide layers were formed on the samples which were placed nearer to the outer part of the quartz tube (see section 3.1.), and thus, the inner samples could absorb more hydrogen which can be seen in the mass gain results of the E110 samples (Fig. 10).

The differences in mass gain were found not to be so big for the Zircaloy-4 samples even at higher temperatures (Fig. 11).

For every temperature an average mass gain was calculated for the four samples that is useful when comparing it to the calculated approximate average amount of absorbed hydrogen (see section 3.4.).

Table 2
Comparison of the mass gain and the quantitative hydrogen content results.

	AHG-21	AHG-24	ZryH-9	ZryH-12
mass gain (ppm)	1279	669	2371	1410
H content by ELTRA (ppm)	1310	616	2586	1447

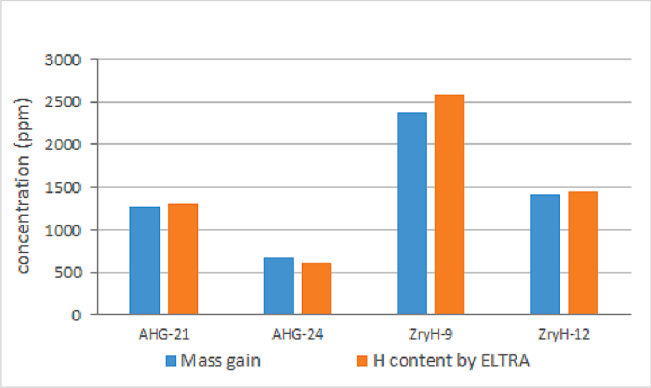

Fig. 12. The mass gain and the results of the quantitatively hydrogen content determination.

3.4. H content results

Approximate calculations were made to estimate the total amount of hydrogen absorbed by the four samples placed at once in the furnace. These calculations were made based on the total pressure decreasing during the measurement (see more detailed description in section 2.3.).

The results of the average hydrogen contents together with the average mass gain results for comparison are summarized in Table 1.

It can be seen that the differences between the calculated average hydrogen content and the mass gain results are under 5 % in every case.

The differences are resulted mainly by the slight oxidation of the samples. The absorbed hydrogen content was calculated based on the pressure decreasing which can also be caused by a slight leakage of the hydrogen from the system during the measurement. It should be noted that it can result overestimations in hydrogen contents.

Two E110 and two Zircaloy-4 samples were chosen for quantitative hydrogen content determination carried out by an elemental analyzer device ELTRA. All of these four samples were hydrogenated at 330 °C, and thin oxide layers were formed on some of them (Fig. 6). The results together with the mas gain of those samples are summarized in Table 2 and Fig. 12.

No significant differences can be seen in the results. In the case of the sample AHG-24 the surplus in the mass gain can be explained by the oxide layer which was also taken into account at the weighing, but three out of the four comparisons show higher hydrogen content than mass gain. It can be explained as follows.

The samples were cut into small (0.03–0.1 g) pieces for the measurement as hot extraction process required only a very small amount of samples. When trying to cut the ring samples they much more easily break at the points where the alloy became more brittle caused by the local higher hydrogen content, and therefore some pieces contain averagely more hydrogen than the average for the whole ring sample. In some cases, with such non-representative pieces selected randomly to be measured, a higher hydrogen content was resulted than the mass gain, however the whole ring sample may contain less hydrogen.

4. Creating and developing a numerical model

The Zircaloy-4 data have already been used for the assessment of hydride precipitation modelling across fuel cladding by Feria and

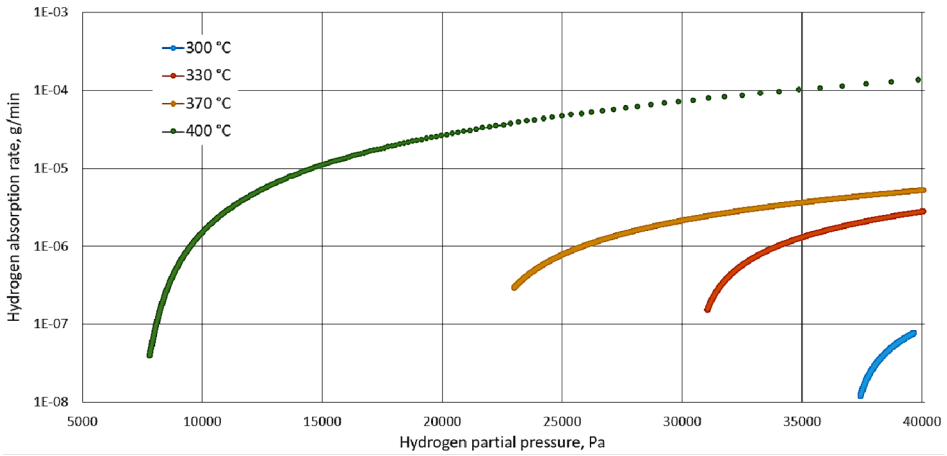

Fig. 13. The hydrogen absorption rate as a function of the hydrogen partial pressure at different temperatures.

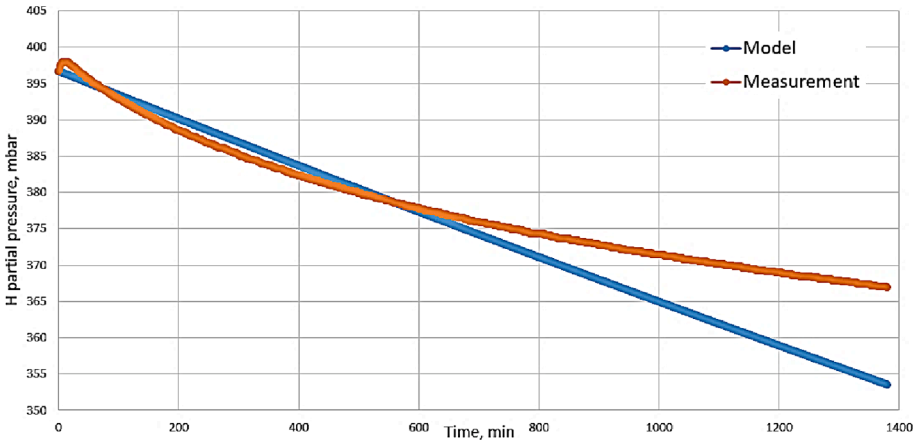

Fig. 14. Comparison of the calculated pressure history and the experimental data at 300 °C.

Herranz (Allen et al., 2012) by implementing a hydrogen uptake correlation in the HYDCLAD code.

Based on E110 the experimental data, a simple model was created to evaluate the hydrogen uptake rate in order to improve the H uptake model in the TSKGO code (Feria and Herranz, 2023), which was developed for the simulation of defective fuel rods. The original hydrogen uptake model had a constant rate value as function of time and was limited by the available amount of hydrogen in the gas volume of the fuel rod. With the introduction of a new model, it was intended to take into account the local temperature and partial pressure, which could create a more realistic kinetics. The TSKGO code simulates the iodine spiking phenomenon in a mechanistic way. The amount of non-condensable gases inside of the fuel rod highly influences the activity release, for this reason the available hydrogen in the gas volume is a key parameter for the simulation.

During the fitting of the parameters of the new correlation the

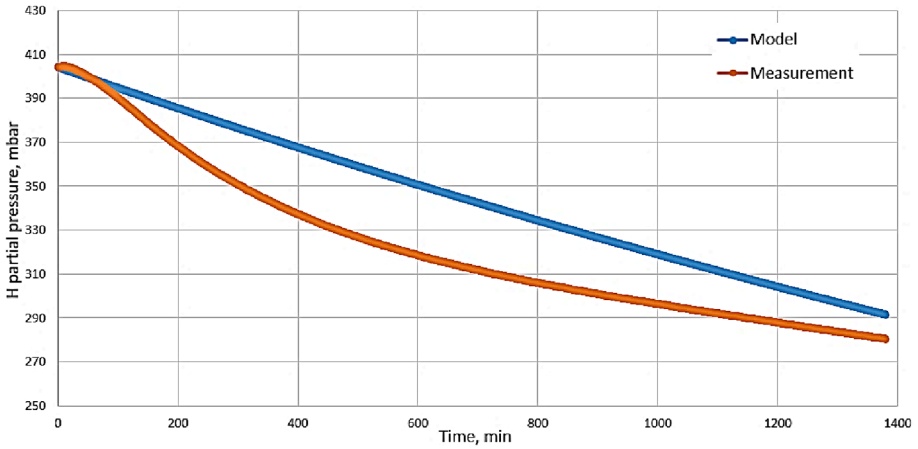

Fig. 15. Comparison of the calculated pressure history and the experimental data at 330 °C.

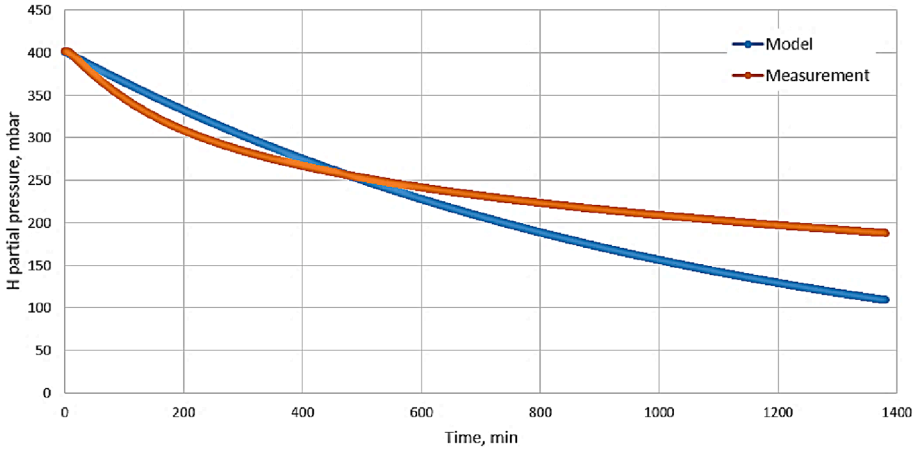

Fig. 16. Comparison of the calculated pressure history and the experimental data at 370 °C.

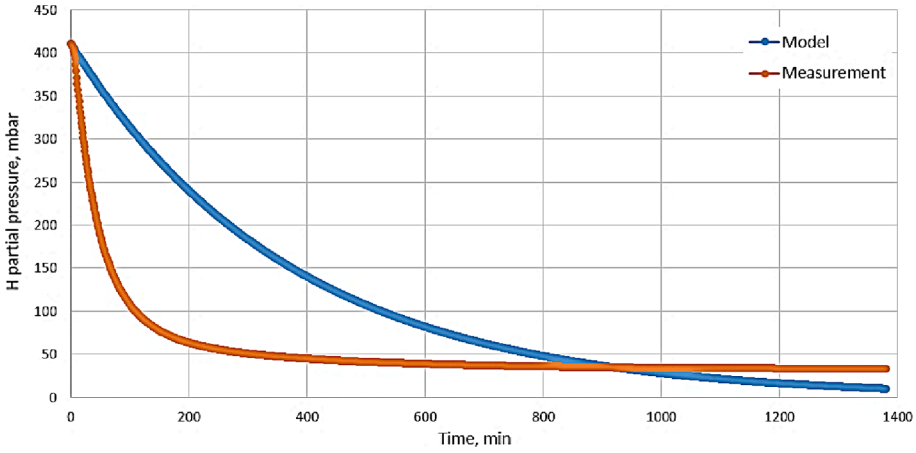

Fig. 17. Comparison of the calculated pressure history and the experimental data at 400 °C.

calculated pressure history was compared to the experimental data. The following requirements were taken into account during the development:

- The model should cover the temperature range of 300–400 °C and the pressure range of 0–400 mbar.
- The model should use a simple formula.
- The correlation should calculate the hydrogen uptake rate based both on the actual temperature and the partial pressure of the hydrogen gas.

In the first step, using the partial pressure history the hydrogen content in the E110 ring samples was calculated for each time step. Four correlations were determined for the four temperatures of the experimental series. The correlations described the amount of the absorbed hydrogen per unit time as function of partial pressure of the hydrogen gas (Fig. 13).

In the second step, the temperature dependence was introduced using an exponential expression. The calculations were repeated for the whole dataset and the pressure and temperature coefficients were fitted by minimizing the difference between calculated and measured data.

The following formula was finally created:

$$dw = A \bullet p_H(t) \bullet e^{B \bullet T}$$

where:

dw hydrogen uptake rate $(g \bullet min^{-1})$.

A pressure constant,.7.5 $\bullet\ 10^{-14} g \bullet min^{-1} \bullet mbar^{-1}$

$p_H(t)$ actual partial pressure of hydrogen *(mbar)*.

B temperature constant, 0.0345°C^{-1}.

T temperature (°C).

This simple formula with the above mentioned values for the constants A and B can give the decentest results to cover the temperature range from 300 to 400 °C. It can be seen that at 300 °C (Fig. 14) and at 330 °C (Fig. 15) the model resulted almost a linear pressure history, however the differences were modest.

It can be seen at 370 °C (Fig. 16) that the model calculated lower hydrogen uptake rates at higher hydrogen partial pressure while the hydrogen uptake coefficient has been overestimated at lower partial pressure values. It is even more noticeable in the case of 400 °C (Fig. 17).

Using the correlation, the total amount of the absorbed hydrogen in the samples was calculated for the experimental conditions at each temperature. Table 3 summarizes the mass gain values given by the model and the calculated mass gains based on the experiments. It can be

Table 3
The calculated and the measured hydrogen content of the samples.

Temperature (°C)	Calculated hydrogen content(ppm)	Measured average hydrogen content(ppm)
300	319	221 ± 20
330	825	907 ± 250
370	2131	1556 ± 400
400	2887	2746 ± 1000

concluded that the values calculated by the model are higher in 3 cases out of 4 as the model is slightly conservative.

5. Summary and conclusions

The experimental series with hydrogen charging of Zircaloy-4 and E110 alloys were successfully completed in the laboratories of Centre for Energy Research.

- The tests covered the temperature range of 300–400 °C and pressure range up to 410 mbar.
- The experimental data showed the increase of hydrogen uptake with the increase of temperature.
- The hydrogen uptake of the two tested alloys was significantly different, probably due to their different composition and alloying elements. Comparing the two alloys' hydrogen uptake at different temperatures we can see that at 300 °C, 330 °C and 370 °C the E110 samples showed lower tendency to absorb hydrogen, however at 400 °C the hydrogen uptake was quicker in the case of the E110 alloy.
- The experimental data provided information on the H uptake rate as function of temperature and partial pressure.

Using the results of E110 experiments, a correlation was created. Using this correlation the experimental data were well reproduced and the correlation can be used for the simulation of H uptake in defective fuel rods.

CRediT authorship contribution statement

P. Szabó: Formal analysis, Investigation, Visualization, Writing – original draft, Writing – review & editing. **Z. Hózer:** Conceptualization, Writing – original draft, Writing – review & editing. **E. Perez-Feró:** Investigation. **T. Novotny:** Investigation, Methodology.

Declaration of competing interest

The authors declare that they have no known competing financial interests or personal relationships that could have appeared to influence the work reported in this paper.

Data availability

No data was used for the research described in the article.

Acknowledgements

This project has received funding from the Euratom research and training programme through the R2CA Project under Grant Agreement no 847656. Views and opinions expressed in this paper reflect only the author's view and the European Commission is not responsible for any use that may be made of the information it contains.

References

Manual ELTRA ELEMENTRAC ONH-p series, Eltra GmbH, 28.07.2017, Version 0005.
Allen, T.R., Konings, R.J.M., Motta, A.T., 2012. 5.03 corrosion of zirconium alloys. Comprehensive Nuclear Materials 5, 49–68.
Couet, A., Motta, A. T., & Comstock, R. J. (2013). Effect of alloying elements on hydrogen pick-up in zirconium alloys. In 17th International Symposium on Zirconium in the Nuclear Industry, ASTM STP (Vol. 1543, pp. 479-514).
Cox, B., 1999. A mechanism for the hydrogen uptake process in zirconium alloys. J. Nucl. Mater. 264 (3), 283–294.
Ensor, B., Lucente, A.M., Frederick, M.J., Sutliff, J., Motta, A.T., 2017. The role of hydrogen in zirconium alloy corrosion. J. Nucl. Mater. 496, 301–312.
Feria, F., Herranz, L.E., 2023. Assessment of hydride precipitation modelling across fuel cladding: Hydriding in non-defective and defective fuel rods. Ann. Nucl. Energy 188, 109810.
Große, M., Steinbrück, M., Lehmann, E., Vontobel, P., 2008. Kinetics of hydrogen absorption and release in zirconium alloys during steam oxidation. Oxid. Met. 70, 149–162.
Grosse, M., van den Berg, M., Goulet, C., Lehmann, E., Schillinger, B., 2011. In-situ neutron radiography investigations of hydrogen diffusion and absorption in zirconium alloys. Nucl. Instrum. Methods Phys. Res., Sect. A 651 (1), 253–257.
Gulbransen, E.A., Andrew, K.F., 1954. Mechanism of the Reaction of Hydrogen with Zirconium: I. Role of Oxide Films, Pretreatments, and Occluded Gases. J. Electrochem. Soc. 101 (7), 348.
Hatano, Y., Isobe, K., Hitaka, R., Sugisaki, M., 1996. Role of Intermetallic Precipitates in Hydrogen Uptake of Zircaloy-2. J. Nucl. Sci. Technol. 33 (12), 944–949.
Lewis, B.J., Iglesias, F.C., Postma, A.K., Steininger, D.A., 1997. Iodine spiking model for pressurized water reactors. J. Nucl. Mater. 244 (2), 153–167.
Novotny, T., Perez-Feró, E., & Horváth, M. (2015). Hydrogenation and high temperature oxidation of Zirconium claddings. In Mitev, M. (Ed.). 11 International Conference on WWER Fuel Performance, Modelling and Experimental Support Proceedings, (p. 712). Bulgaria.
Olander, D.R., Kim, Y.S., Wang, W.E., Yagnik, S.K., 1999. Steam oxidation of fuel in defective LWR rods. J. Nucl. Mater. 270 (1–2), 11–20.
Seo, S.B., Duchnowski, E.M., O'Neal, M., Motta, A.T., Passelaigue, F., Kang, S., Pastore, G., Manera, A., Petrov, V., Huang, P.H., Brown, N.R., 2021. Sensitivity analysis of BISON model for characterization of impact of experimental parameters on hydrogen migration and redistribution in zirconium-based alloys. J. Nucl. Mater. 550, 152941.
Steinbrück, M., 2004. Hydrogen absorption by zirconium alloys at high temperatures. J. Nucl. Mater. 334 (1), 58–64.
Suman, S., Khan, M.K., Pathak, M., Singh, R.N., Chakravartty, J.K., 2015. Hydrogen in Zircaloy: Mechanism and its impacts. Int. J. Hydrogen Energy 40 (17), 5976–5994.
Szabó, P., Hózer, Z., Kulacsy, K., Somfai, B., Nagy, R., Burján, T., Baracska Varjú, I., Pintér, T., 2017. Numerical simulation of the telescope sipping of a leaking VVER fuel assembly. Ann. Nucl. Energy 99, 345–352.
Une, K., Imamura, M., Amaya, M., Korei, Y., 1995. Fuel oxidation and irradiation behaviors of defective BWR fuel rods. J. Nucl. Mater. 223 (1), 40–50.
Veshchunov, M.S., Shestak, V.E., 2012. Models for hydrogen uptake and release kinetics by zirconium alloys at high temperatures. Nucl. Eng. Des. 252, 96–107.
Wright, J., Tverberg, T., Yagnik, S., Limbäck, M., & Schrire, D. (2017, September). Summary of test reactor experiments to simulate secondary fuel degradation and its mitigation. In 2017 Water Reactor Fuel Performance Meeting (TopFuel-2017).